

A method for the temperature calibration of an infrared camera using water as a radiative source

S. M. Bower, J. Kou, and J. R. Saylor

Department of Mechanical Engineering, Clemson University, Clemson, South Carolina 29634-0921, USA

(Received 29 June 2009; accepted 6 August 2009; published online 10 September 2009)

Presented here is an effective low-cost method for the temperature calibration of infrared cameras, for applications in the 0–100 °C range. The calibration of image gray level intensity to temperature is achieved by imaging an upwelling flow of water, the temperature of which is measured with a thermistor probe. The upwelling flow is created by a diffuser located below the water surface of a constant temperature water bath. The thermistor probe is kept immediately below the surface, and the distance from the diffuser outlet to the surface is adjusted so that the deformation of the water surface on account of the flow is small, yet the difference between the surface temperature seen by the camera and the bulk temperature measured by the thermistor is also small. The benefit of this method compared to typical calibration procedures is that, without sacrificing the quality of the calibration, relatively expensive commercial blackbodies are replaced by water as the radiative source ($\varepsilon \approx 0.98$ for the wavelengths considered here). A heat transfer analysis is provided, which improves the accuracy of the calibration method and also provides the user with guidance to further increases in accuracy of the method. © 2009 American Institute of Physics.

[doi:10.1063/1.3213075]

I. INTRODUCTION

Infrared (IR) cameras offer a means by which spatial variations in temperature can be measured, providing a temperature field which cannot be obtained from single-point radiation thermometers such as pyrometers. Such temperature measurements are of great utility in many applications including machine tooling and manufacturing processes,^{1,2} flow visualizations,^{3–5} astronomy, oceanographic⁶ and atmospheric studies, and medical research.^{7,8} To obtain accurate temperature measurements from these devices, a temperature calibration is required where the device output is compared to a temperature reference. General methods for thermometric calibration are many, and since space limitations preclude a full review of prior work, only those methods immediately relevant to IR cameras will be presented here.

An IR camera is typically calibrated by imaging a target surface over a range of known temperatures. The range of calibration temperatures ideally extends beyond the range of temperatures, which are to be measured during experiments or application. The relationship between the camera gray level and the target surface temperature can then be used in the form of a look-up table or a curve fit to the data.

The gray level output g of the IR camera is dependent upon the spectral blackbody radiation $M(\lambda, T)$ emitted by the source at temperature T , the spectral emissivity of the source $\varepsilon(\lambda)$, and the sensitivity and response characteristics of the IR detector $D(\lambda)$.^{9,10} The sensitive waveband of the detector dictates the limits of integration λ_1 and λ_2 . Following the basic scheme of Kiwamoto *et al.*,⁹ the gray level is given by

$$g(T) = \int_{\lambda_1}^{\lambda_2} \varepsilon(\lambda) M(\lambda, T) D(\lambda) d\lambda. \quad (1)$$

Directional effects have not been included in Eq. (1), and thus it is assumed that the radiated energy is diffuse. A simplification can be made to Eq. (1) by using the average emissivity $\bar{\varepsilon}$ over the detector waveband. This simplification is reasonable if the emissivity of the target surface does not vary significantly within the sensitive waveband. Thus, the camera will have a gray level output when viewing the target surface at temperature T_s of

$$g(T_s) = \bar{\varepsilon} \int_{\lambda_1}^{\lambda_2} M(\lambda, T_s) D(\lambda) d\lambda = \bar{\varepsilon} g_B(T_s), \quad (2)$$

where $g_B(T_s)$ is the response for a blackbody surface ($\bar{\varepsilon}=1$) at temperature T_s . By assuming that the radiative source is opaque (transmissivity, $\tau=0$), the reflectivity can be shown via the Helmholtz relationship to be $\bar{\rho}=1-\bar{\varepsilon}$. The radiation from the ambient (assumed to be black and at a uniform temperature of T_∞) reflected from the target surface will thereby yield a detector response of

$$g(T_\infty) = (1 - \bar{\varepsilon}) \int_{\lambda_1}^{\lambda_2} M(\lambda, T_\infty) D(\lambda) d\lambda = (1 - \bar{\varepsilon}) g_B(T_\infty). \quad (3)$$

The total response of the camera is comprised of radiation from both the target surface and the reflected background,

$$g(T_s, T_\infty) = g(T_s) + g(T_\infty) = \bar{\varepsilon} g_B(T_s) + (1 - \bar{\varepsilon}) g_B(T_\infty). \quad (4)$$

The goal of IR camera calibration is to determine the relationship between the blackbody camera response g_B and

temperature T . This can be achieved experimentally by observing a target surface at a range of known temperatures T_s . The blackbody camera response to the imposed temperature can be found by rearranging Eq. (4) to give

$$g_B(T_s) = \frac{1}{\bar{\epsilon}} [g(T_s, T_\infty) - (1 - \bar{\epsilon})g_B(T_\infty)]. \quad (5)$$

Here, the quantity $g(T_s, T_\infty)$ is measured with the IR camera. The term $g_B(T_\infty)$ is not immediately known, but can be determined in one of two ways: (1) computationally where Eq. (5) is solved iteratively and $g_B(T_\infty)$ is updated between iterations until a convergence criterion is met or (2) experimentally where a uniform surface at exactly room temperature T_∞ is imaged such that Eq. (4) reduces to $g(T_\infty, T_\infty) = \bar{\epsilon}g_B(T_\infty) + (1 - \bar{\epsilon})g_B(T_\infty) = g_B(T_\infty)$. The representation of Eq. (5) may be in the form of a table of numbers giving g_B and T_s or as an empirical fit to the calibration data. Additionally, this relation may be obtained by either averaging the response over all of the pixels in the camera (i.e., a single calibration function for the camera) or by obtaining a separate version of Eq. (5) for each pixel in the detector array to account for spatial variations in the detector.

While the basic scheme for conducting a calibration is relatively straightforward as outlined in Eqs. (1)–(5), the facilities in which the calibrations are conducted are many and varied. A practical guide to thermometry with an IR camera is given by Cetas¹⁰ who discusses a calibration procedure with a thermal cavity. Several other researchers have also utilized a temperature controlled cavity to approximate blackbody surface behavior for the calibration of both IR cameras and radiometric devices alike.^{5,11–15} Conover and Saylor⁵ constructed a thermal cavity for the calibration of a cooled-chip platinum silicide focal plane array (FPA) detector sensitive to wavelengths in the 3.5–5 μm band. The inside of the cavity was coated with high emissivity paint and the apparatus was placed in a water bath to control the temperature. Rainieri and Pagliarini¹² fabricated a copper cylindrical cavity for the calibration of a platinum silicide detector sensitive to the 3.6–5 μm range. Embedded thermocouples were used to obtain temperature measurements over the range of 10–70 $^\circ\text{C}$. Machin and Chu¹⁵ designed three similar blackbody cavity devices, which were regulated with heat pipes using ammonia, water and cesium, and sodium as the different working fluids. These cavities provided blackbody temperatures ranging from -40 to 50 $^\circ\text{C}$, 50–600 $^\circ\text{C}$, and 500–1000 $^\circ\text{C}$, respectively, at $\epsilon > 0.999$. Ma and Bedford¹⁴ discuss the optimal design of such a cavity as a blackbody source.

Particular consideration should be given to the material used as the target surface during a calibration. Many of the aforementioned researchers used facilities constructed of solid copper, for example. Water is a particularly useful calibration source since it is readily available, and its optical properties are well documented.^{16–19} For these reasons, it has been utilized by several researchers as a quasiblackbody surface during calibration procedures.^{6,20} Horwitz²⁰ notes that water is an ideal calibration source specifically since (1) its vapor phase is nontoxic, (2) its vapor phase does not absorb significant radiation in the middle infrared range at path

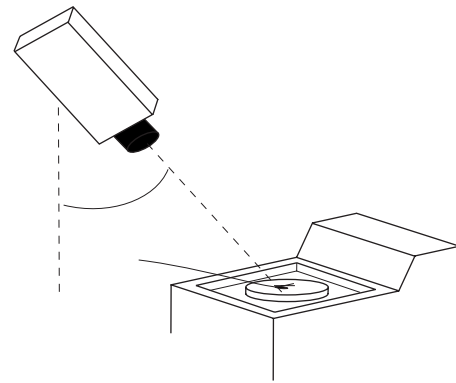


FIG. 1. Schematic of the calibration facility consisting of the temperature controlled water bath, tripod-mounted IR camera, the diffuser apparatus (detailed in Fig. 2), submersible pump, and thermistor probe.

lengths typical of calibrations, (3) the liquid phase is opaque and provides a favorably high emissivity ($\epsilon \approx 0.98$) in the middle infrared range, and (4) its melting point is a temperature that is useful to the experimenter (especially since most commercial blackbodies are usually not reliable at or around ambient temperature). Horwitz²⁰ exploited the freezing point of water to serve as a temperature standard for thermometric devices by creating an ice bath mixture with distilled water and imaging the floating ice cubes with an IR camera sensitive to the 8–13.5 μm wavelength band.

The method presented herein was motivated by the need to calibrate an IR camera with an accurate, practical, and relatively low-cost facility. Specifically, the authors are concerned with experiments in which the surface temperature field of an air/water interface undergoing natural convection must be measured. By exploiting the favorable infrared properties of water, this method proves to be a cost-effective alternative to commercial blackbodies without sacrificing the quality of the calibration.

II. CALIBRATION METHOD

The calibration facility is presented in Fig. 1, and consists of a diffuser apparatus and a submersible pump all of which are located within a constant temperature water bath. Water is pumped from the water bath into the diffuser apparatus, which is illustrated in Fig. 2, creating an upwelling flow toward the surface. The temperature of the flow is measured with a thermistor located just beneath the surface. At the surface, the water flows radially outward from the center and spills back into the temperature controlled water bath. The IR camera is mounted above the water surface so that the center of the IR image is the position of the water surface located just above the thermistor probe. Broadly speaking, the calibration is obtained by recording the intensities of those pixels imaging the region of the water surface just above the thermistor location, and correlating these gray levels to the thermistor temperature measurement. The strength of this method is that the temperature of the fluid, which is imaged by the IR camera, is measured by a probe, which is located just beneath the surface and in the upwelling flow. Hence a very short period of time elapses between the measurement of the water temperature and the imaging of that

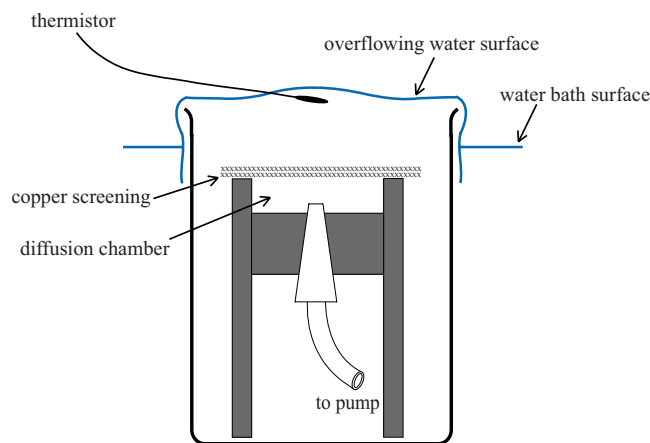


FIG. 2. (Color online) Illustration of the diffuser apparatus, which resides almost entirely submerged in the water bath. After entering the diffuser chamber, the water flow passes through copper screening and continues toward the surface. At the surface, the flow moves radially outward and spills over the edge of the beaker back into the heated water bath.

fluid. This helps ensure that any change in the fluid temperature away from the thermistor temperature, due to heat transfer with the environment, is small (although a correction obtained from a thermal analysis is presented later to account for this change). This method is superior to approaches where a thermistor is located right at the air/water interface, since in that approach, the thermistor is exposed to air and the measurement would be affected by the air temperature. Increasing the flow velocity leaving the diffuser, and/or moving the diffuser closer to the water surface, both serve to reduce the time interval between measurement of the fluid temperature by the thermistor and imaging of that fluid at the surface. However, this also serves to deform the water surface, which degrades accuracy. A tradeoff between these two exists, and the parameters presented below for these variables represent optimum values obtained by trial-and-error.

It is noted that in Fig. 1, the camera is mounted at an angle of 25° from vertical and with the camera lens 625 mm from the water surface of the diffuser apparatus. The purpose for orienting the camera at an angle was to ensure that the resulting calibration was valid for a separate experimental study²¹ conducted by the authors, where the same geometry was used. When implementing this method, the camera, ideally, should be oriented at a distance and angle from the surface identical to that of the actual application.

The calibration method was tested on an M-Wave IR camera (model MW320F4 $f/2.3$ from IR Cameras Infrared Imaging Systems). The camera detector was a 320×240 Stirling cycle cooled indium antimonide (InSb) FPA sensitive to the $3\text{--}5\ \mu\text{m}$ range with a noise equivalent differential temperature of 0.015 K. The camera was outfitted with a 25 mm lens resulting in a $21^\circ \times 16.8^\circ$ ($H \times V$) field of view. The temperatures of the room air and the upwelling water flow, respectively, were measured with a General Electric CSP60BA103M-H/2–90 thermistor and a Fluke 5611 T thermistor (both accurate within $\pm 0.01^\circ\text{C}$) and logged with a Hart Scientific 1529 Chub-E4 thermometer readout ($\pm 0.002^\circ\text{C}$ accuracy). The water thermistor probe (2.5 mm in diameter and 10 mm in length) was located 2 mm below

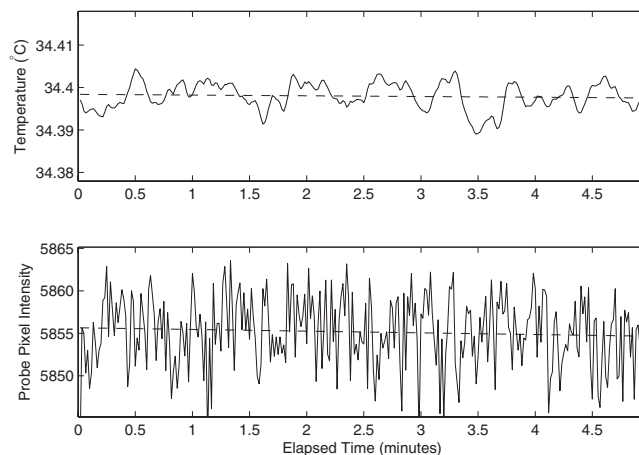


FIG. 3. Sample calibration data for a single temperature of 34.4°C . The upper plot is the probe temperature, and the lower plot is the gray level output from the camera. The dashed lines are both linear fits to the data for the duration of the run.

the water surface at the center of the upwelling flow as illustrated in Fig. 2. The average room air temperature in the laboratory was 23.26°C and the average relative humidity was 35% (measured with a digi-sense thermohygrometer with an accuracy of $\pm 0.2\%$ of reading). A Brinkmann Lauda type RMT6 recirculating water bath (9 L/min) was used to control the water temperature and house the diffuser apparatus and submersible pump. This diffuser apparatus consisted of a 600 mL glass beaker (95 mm diameter, 125 mm height), the lip of which was located 1 cm above the water level of the water bath. Inside of the beaker was the diffuser assembly, which had a diameter of 35 mm. The outlet of the diffuser chamber was covered with two layers of copper screen (7 mm above the inlet to the diffuser chamber). The purpose of this screen cover was to provide fluidic resistance such that the velocity profile at the diffuser outlet was nearly uniform, and so that the surface would be only slightly deformed (the water surface near the stagnation region bulged approximately 4 mm above the quiescent water surface). A rigid structure held the diffuser outlet 13 mm below the top of the beaker. A 16.5 in. length of flexible tubing (5 mm inside diameter) connected the diffuser apparatus with a Peaktop Ltd. 120 V submersible fountain pump model MD80. The flow rate through the diffuser was 23.2 mL/s.

When testing this method, the water bath was set to the initial calibration temperature and the submersible pump was turned on. The system was given 30 min to stabilize before the first set of calibration data was taken. For subsequent temperature set-points (incremented by approximately 1.5°C), a period of 20 min was allowed for the water bath temperature to stabilize. For each set-point, IR imagery and thermistor temperature data were collected at a rate of 1 Hz for 5 min. It is noted that the camera was calibrated to the thermistor temperature, averaged over the 5 min of data collection. This temperature typically deviated slightly from the water bath set point. An example of the thermistor probe temperature data and corresponding image intensity values from the camera are shown in Fig. 3.

Since the thermistor probe measurements report the av-

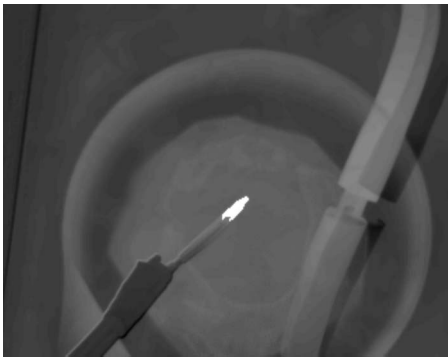


FIG. 4. The difference image showing the probe pixels in white. This image was obtained by subtracting an image obtained with the probe submerged from an image with the beaker apparatus drained.

erage temperature of the water flowing around the probe, it is important to find the average gray level intensity of only those pixels in the IR imagery located directly above the thermistor probe. The locations of these probe pixels were identified by acquiring two reference images. This was done by taking an image while the submersible pump was still turned on, and taking a second image with the submersible pump off and the water drained from the diffuser apparatus beaker (i.e., the thermistor probe was no long submerged). By subtracting these two images, the pixels giving the sub-surface location of the thermistor probe during the calibration procedure were easily identified, as shown in Fig. 4 where a sample difference image is presented. The (i, j) locations of the probe pixels (exactly 134 pixels in this case) were identified and recorded, and in subsequent data processing the intensities of these pixels were averaged to provide a single gray level for each image. It is this average gray level, which is plotted in the lower plot of Fig. 3.

A finite amount of heat transfer occurs at the water surface as fluid travels radially outward from the center of the beaker to the location above the edge of the thermistor probe (i.e., from the center to the edge of the group of probe pixels highlighted in Fig. 4). Accordingly, the temperature measured with the thermistor probe is not exactly the same as the temperature at the water surface. This small error can be corrected via a heat transfer analysis, which is presented in Sec. III. This correction is used to correct (reduce) the measured probe temperature, and it is this corrected probe temperature that is used to develop the calibration according to Eq. (5). That is, the value of T_s used in Eq. (5) is

$$T_s = T_p - \Delta T, \quad (6)$$

where T_p is the temperature measured by the probe, and ΔT is the probe correction, which is developed in Sec. III. These corrected probe temperatures are plotted against the average intensities of the probe pixels for each temperature set-point in Fig. 5. These data were fitted with a fourth order polynomial to obtain a calibration function which, for the camera and calibration setup developed here, was

$$T(g) = (-3.9998 \times 10^{-16})g^4 + (2.7569 \times 10^{-11})g^3 - (7.9128 \times 10^{-7})g^2 + (0.0129)g - (19.3471) \quad (7)$$

for temperatures ranging from 30–65 °C. Calibration curves

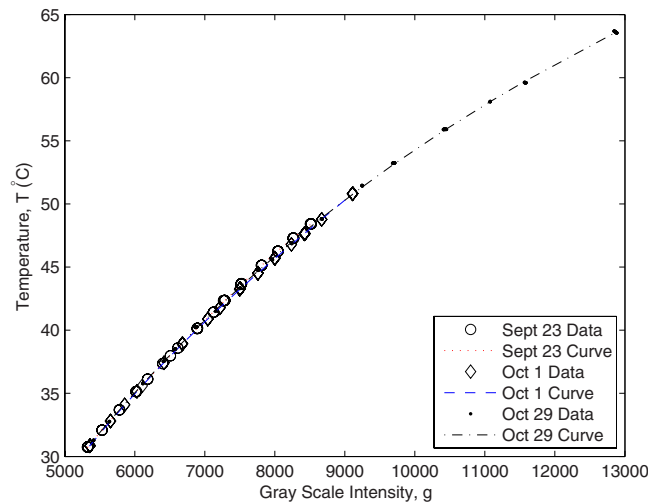


FIG. 5. (Color online) Calibration curves from three different dates relating the 14-bit gray scale intensity values to temperature. The two earliest calibrations cover temperatures ranging from 30–50 °C while the latest calibration was conducted from 30–65 °C.

of three calibrations for the same camera on different days are shown in Fig. 5. The October 29 calibration represented in Eq. (7) was conducted for a larger range of temperatures than the two earlier calibrations. For the 30–50 °C temperature range, the standard deviation of the three calibration curves from an average fit to the data is ± 0.0995 °C. An error analysis²² was conducted to account for measurement accuracy (temperature probes, thermohygrometer, and camera noise) and data processing (standard deviations of fits to the data). With respect to the specific instrumentation and setup presented here, the calibration curves have an uncertainty of ± 0.1805 °C. The deviation of the three calibrations in the 30–50 °C range in Fig. 5 is less than the value of the calibration accuracy, which demonstrates favorable repeatability of the described calibration method.

III. THERMAL ANALYSIS

The magnitude of ΔT in Eq. (6) is due to evaporation, natural convection heat transfer from the surface to the air, and radiation heat transfer from the water surface to the room walls. This heat transfer occurs during the time t_f required for the fluid to travel from the location of the thermistor probe beneath the water surface to the location at the water surface above the edge of the probe. This temperature drop is computed by performing an energy balance on a fluid parcel as it travels this distance. The fluid parcel has a volume δ^3 (the temperature within is assumed to be uniform) as indicated in Fig. 6. The sum of the four energy transfers indicated in Fig. 6 (evaporative, convective, radiative and conductive), sum to provide the net heat loss by the parcel, \dot{q} , which can be related to the time rate of change in temperature dT/dt via the equation:

$$\dot{q} = \rho c_p V \frac{dT}{dt}, \quad (8)$$

where ρ and c_p are the density and specific heat of water, respectively, and V is the volume δ^3 . Equation (8) can be rearranged and integrated to give the drop in temperature of

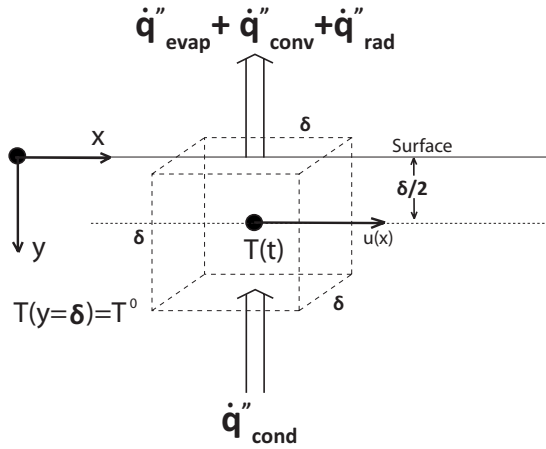


FIG. 6. Diagram of the finite volume of fluid as it travels along the surface away from the stagnation point.

the fluid parcel, which is the correction to the probe temperature,

$$\Delta T = T(t_f) - T(0) = \frac{1}{\rho c_p V} \int_0^{t_f} \dot{q} dt. \quad (9)$$

Replacing \dot{q} with its component heat fluxes gives

$$\Delta T = T(t_f) - T(0) = \frac{1}{\rho c_p \delta} \int_0^{t_f} [\dot{q}''_{\text{evap}} + \dot{q}''_{\text{conv}} + \dot{q}''_{\text{rad}} + \dot{q}''_{\text{cond}}] dt. \quad (10)$$

In this analysis, the conduction heat transfer is through the bottom of the control volume and the conduction heat transfer through the sides of the volume is assumed to be negligible.

The evaporative heat flux is

$$\dot{q}''_{\text{evap}} = \dot{m}'' h_{fg} = h_m (\rho_{wv,s} - \gamma \rho_{wv,\infty}) h_{fg}, \quad (11)$$

where the density of water vapor in the ambient and at the surface are given by $\rho_{wv,\infty}$ and $\rho_{wv,s}$, respectively, where γ is the relative humidity and h_{fg} is the latent heat of vaporization of water. The mass transfer coefficient, h_m , is obtained from the Sherwood–Rayleigh (Sh–Ra) power law scaling due to Bower and Saylor,²¹

$$\text{Sh} = 0.230 \text{Sc}^{1/3} \text{Ra}_m^{0.321}, \quad (12)$$

where

$$\text{Sh} = \frac{h_m W}{D}. \quad (13)$$

Here, W is the characteristic length (diameter) of the beaker, D is the diffusion coefficient for water vapor in air, and Ra is the Rayleigh number given by

$$\text{Ra} = \frac{g \Delta \rho W^3}{\bar{\rho} \nu \alpha}, \quad (14)$$

where g is the acceleration due to gravity, $\Delta \rho$ is the difference between the air/water vapor mixture density at the surface and in the ambient, $\bar{\rho}$ is the average air/water vapor mixture density between the surface and ambient, and ν and

α are the kinematic viscosity and thermal diffusivity of air, respectively.

The convective heat flux is

$$\dot{q}''_{\text{conv}} = h(T_s - T_\infty), \quad (15)$$

where the heat transfer coefficient h is obtained from the Nusselt–Rayleigh (Nu–Ra) power law scaling for natural convection over a heated plate,²³

$$\text{Nu}_L = 0.54 \text{Ra}_L^{1/4}, \quad (16)$$

where

$$\text{Nu}_L = \frac{hL}{k}, \quad (17)$$

L is the ratio of the beaker surface area to the perimeter of the beaker, k is the thermal conductivity of air, and Ra_L is defined differently from Eq. (14),

$$\text{Ra}_L = \frac{g \beta (T_s - T_\infty) L^3}{\nu \alpha}. \quad (18)$$

Here, β is the coefficient of thermal expansion of air, and ΔT is the temperature difference between the water surface and the ambient.

The radiative heat flux is

$$\dot{q}''_{\text{rad}} = \sigma \bar{\epsilon} (T_s^4 - T_\infty^4), \quad (19)$$

where σ is the Stefan–Boltzmann constant and $\bar{\epsilon}$, as previously defined, is the average emissivity over the sensitive range of the IR camera.

Finally, the conduction heat flux into the fluid parcel from the underlying fluid can be calculated using Fourier's law,

$$\dot{q}''_{\text{cond}} = -k \frac{dT}{dy}. \quad (20)$$

Here, the derivative dT/dy is discretized and Eq. (20) is rewritten as:

$$\dot{q}''_{\text{cond}} = -k \frac{T_s - T_p}{\Delta y}, \quad (21)$$

where Δy is the vertical distance from the surface (at temperature T_s) to the depth of the thermistor probe (at this depth, we assume the temperature is uniformly T_p).

The last variable needed to solve Eq. (10) and obtain ΔT is t_f , the time necessary for the fluid parcel to travel from the location of the probe beneath the surface to the location at the water surface over the edge of the probe. This time is obtained by integrating the velocity, which is modeled as a two-dimensional inviscid stagnation point flow, where the upwelling liquid is treated as if it is striking a solid surface. In Cartesian coordinates, the velocity field for this flow is²⁴

$$(u, v) = \left(\frac{\partial \psi}{\partial y}, -\frac{\partial \psi}{\partial x} \right) = \left(\frac{U}{D} x, -\frac{U}{D} y \right), \quad (22)$$

where D is the distance from the diffuser outlet to the surface, and U is the velocity of the flow at the diffuser outlet. The horizontal component of velocity u is integrated by separation of variables to obtain

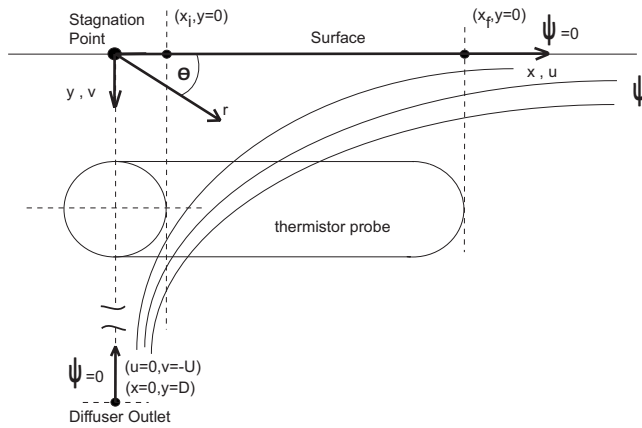


FIG. 7. Schematic of the stagnation point stream with the thermistor probe below the surface. Here, the diffuser outlet is at a depth, D , below the origin where it emits water with a vertical velocity, U . The stream $\psi=0$ corresponds to the flow at both the centerline and at the surface.

$$\ln\left(\frac{x_f}{x_i}\right) = -\frac{U}{D}(t_f - 0), \quad (23)$$

where x_i and x_f are the initial and final horizontal positions of the fluid parcel. These positions, along with the stagnation point flow, are illustrated in Fig. 7. Assuming that the probe is centered underneath the stagnation point, the half-length of the thermistor probe can be assigned as the value for x_f . The value of x_i was chosen to be the radius of the probe, which is a physically meaningful starting location, and which also avoids the mathematical singularity in Eq. (23) if the stagnation point $x=0$ is chosen.

Once the value of t_f is obtained from Eq. (23) (for the apparatus used here, $t_f=0.664$ s), numerical integration is used to solve Eq. (10) with time t being the variable of integration. At each time step, the surface temperature T_s is updated. Solving Eq. (10) with the upper integration limit varied from 0 to t_f yields a temperature profile with respect to surface position (that is, as the parcel travels from the stagnation point position at $t=0$ to the tip-end of the probe at $t=t_f$ we obtain $\Delta T[x(t)]$). The average ΔT along this profile is used to obtain T_s in Eq. (6).

The magnitude of the correction to the probe temperature obtained from the above analysis is presented in Fig. 8, where the adjusted probe temperature is plotted against the measured probe temperature. The correction is small, but not insignificant, varying from a value of 0.1911 °C at 30 °C to 2.017 °C at 66 °C. It should be noted that the results shown in Fig. 8 reflect the temperature corrections for the authors' specific setup and laboratory conditions and are provided here as examples of how the heat transfer analysis affects the surface temperature measurements.

IV. DISCUSSION AND CONCLUSION

The described method is a practical technique for calibrating IR cameras in the range of 0 – 100 °C using water as the radiative source. The heat transfer analysis provides corrections to the measured probe temperatures that are used to calibrate the camera. The calibration is accurate to

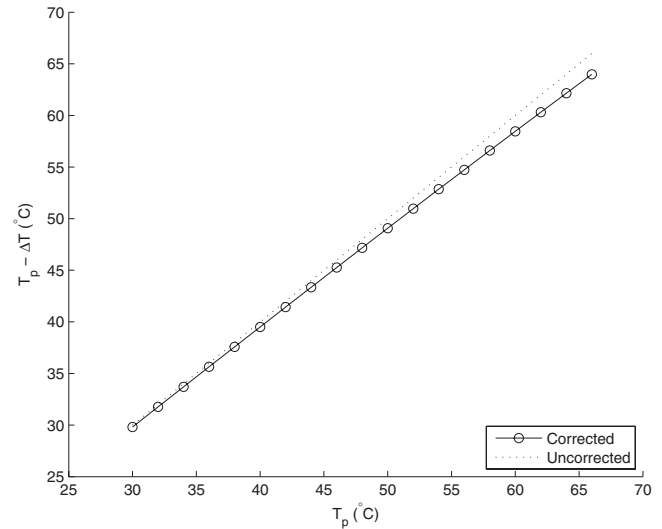


FIG. 8. An example of the adjusted probe temperature as a function of the measured probe temperature computed for $\gamma=35\%$ and $T_\infty=23.26$ °C. The dashed line represents the uncorrected probe temperature.

± 0.1805 °C using the described instrumentation. The present method is thereby a cost-effective means to conduct a calibration of an IR camera with accuracy comparable to that of a commercial blackbody device.

Several actions can be taken to decrease the heat transfer that occurs at the surface, and thereby decrease the temperature correction. The first order of action would be either to increase the velocity of the flow (by increasing the flow rate of the pump or decreasing the cross-sectional area of the diffuser outlet) or decrease the distance between the diffuser outlet and the surface. Either alteration will decrease the amount of time Δt that fluid remains at the surface according to Eq. (23), and thus decrease the magnitude of the resulting heat transfer. Care must be given when increasing the velocity of the flow, however, in order to avoid significantly deforming the flat water surface. While herein the authors have assumed the optical properties of water to be diffused, finite deviations of the observed emitted energy are likely to occur on account of directional effects as the surface changes from flat.

Second, since evaporation was found to be the largest component of the total heat transfer (for the conditions explored here), reduction in this component by increasing the relative humidity γ and ambient temperature T_∞ beyond typical laboratory conditions would improve accuracy by reducing the $\Delta\rho$ terms in Eqs. (11) and (14), and consequently the evaporative heat flux. This could be achieved by enclosing the water bath (perhaps a tightly sealed container with an aperture for the IR camera), which would raise the relative humidity and air temperature within the apparatus. Also, a small air-side heat exchanger could be included inside the enclosure to raise T_∞ without introducing any air flow beyond natural convection conditions. Ideally, if $\gamma=100\%$ and $T_\infty=T_s$, then *no* evaporative heat transfer will occur. Furthermore, the convective and radiation heat transfer will also approach zero as T_s approaches T_∞ in Eqs. (15), (18), and (19).

The nonuniformity of the FPA ought to be considered when using this calibration procedure since the temperature response of a select number of pixels (those located above the thermistor probe) are averaged and subsequently applied to the entire FPA. Provided that the nonuniformity of the FPA is small, this procedure is acceptable, and the authors refer the reader to the work of Marinetti *et al.*²⁵ and Mooney and Shepherd²⁶ who discuss the characterization of noise and nonuniformity of FPAs. If spatial variation of the FPA response is significant, an array of upwelling flows could be used (instead of the single upwelling flow discussed herein) to simultaneously calibrate the different regions of the detector. Alternatively, the camera could be mounted on an x - y stage and several different locations could be calibrated independently to provide a different calibration equation for each region in the array.

While water is particularly convenient to use during calibrations, its practicality is limited to temperatures between its freezing and boiling points. This method is thereby excluded for the calibration of IR cameras at extreme temperatures. However, for applications requiring accurate measurements in the 0–100 °C range, the described method and apparatus are a cost-effective and efficient means of calibrating an IR camera.

ACKNOWLEDGMENTS

Support from the National Science Foundation is gratefully acknowledged.

- ¹J. Hwang, S. Kompella, S. Chandrasekar, and T. N. Farris, *ASME J. Tribol.* **125**, 377 (2003).
- ²M. A. Davies, H. Yoon, T. L. Schmitz, T. J. Burns, and M. D. Kennedy, *Mach. Sci. Technol.* **7**, 167 (2003).
- ³R. J. Volino and G. B. Smith, *Exp. Fluids* **27**, 70 (1999).
- ⁴T. A. Conover and J. R. Saylor, *Langmuir* **22**, 6881 (2006).
- ⁵T. A. Conover and J. R. Saylor, *Exp. Fluids* **43**, 509 (2007).
- ⁶P. Schluessel, W. J. Emery, H. Grassl, and T. Mammen, *J. Geophys. Res.* **95**, 13341, DOI:10.1029/JC095iC08p13341 (1990).
- ⁷B. F. Jones and P. Plassmann, *IEEE Eng. Med. Biol. Mag.* **21**, 41 (2002).
- ⁸E. F. J. Ring, *Infrared Phys. Technol.* **49**, 297 (2007).
- ⁹Y. Kiwamoto, H. Abe, Y. Tatematsu, T. Saito, M. Kurata, K. Kajiwara, Y. Kikuchi, T. Takahashi, and T. Tamano, *Rev. Sci. Instrum.* **68**, 2422 (1997).
- ¹⁰T. C. Cetas, *Rev. Sci. Instrum.* **49**, 245 (1978).
- ¹¹Y. H. Chen, Y. P. Liu, Y. Q. Li, X. Y. Jin, and H. X. Song, *Meas. Sci. Technol.* **12**, 491 (2001).
- ¹²S. Rainieri and G. Pagliarini, *Infrared Phys. Technol.* **43**, 345 (2002).
- ¹³Y. Té, P. Jeseck, C. Camy-Peyret, S. Payan, S. Briaudeau, and M. Fanejeux, *Metrologia* **40**, 24 (2003).
- ¹⁴C. K. Ma and R. E. Bedford, *Rev. Sci. Instrum.* **63**, 3213 (1992).
- ¹⁵G. Machin and B. Chu, *Imaging Sci. J.* **48**, 15 (2000).
- ¹⁶H. D. Downing and D. Williams, *J. Geophys. Res.* **80**, 1656, DOI:10.1029/JC080i012p01656 (1975).
- ¹⁷A. N. Rusk, D. Williams, and M. R. Querry, *J. Opt. Soc. Am.* **61**, 895 (1971).
- ¹⁸D. M. Wieliczka, S. Weng, and M. R. Querry, *Appl. Opt.* **28**, 1714 (1989).
- ¹⁹M. R. Querry, D. M. Wieliczka, and D. J. Segelstein, in *Handbook of Optical Constants of Solids II*, edited by E. D. Palik (Academic, San Diego, 1998).
- ²⁰J. W. Horwitz, *Appl. Opt.* **38**, 4053 (1999).
- ²¹S. M. Bower and J. R. Saylor, *Int. J. Heat Mass Transfer* **52**, 3055 (2009).
- ²²R. S. Figliola and D. E. Beasley, *Theory and Design for Mechanical Measurements*, (Wiley, New York, 1995).
- ²³F. P. Incropera and D. P. DeWitt, *Fundamentals of Heat and Mass Transfer*, 4th ed. (Wiley, New York, 1996).
- ²⁴P. K. Kundu, *Fluid Mechanics* (Academic, New York, 1990).
- ²⁵S. Marinetti, X. Maldague, and M. Prystay, *Mater. Eval.* **55**, 407 (1997).
- ²⁶J. M. Mooney and F. D. Shepherd, *Infrared Phys. Technol.* **37**, 595 (1996).